Defect accommodation in off-stoichiometric (SrTiO3)nSrO Ruddlesden–Popper superlattices studied with positron annihilation spectroscopy

Dawley, Natalie M.; Goodge, Berit H.; Egger, Werner; Barone, Matthew R.; Kourkoutis, Lena Fitting; Keeble, David J.

Published in:
Applied Physics Letters

DOI:
10.1063/5.0011136

Publication date:
2020

Document Version
Peer reviewed version

Defect accommodation in off-stoichiometric $(SrTiO_3)_nSrO$ Ruddlesden-Popper superlattices studied with positron annihilation spectroscopy

Natalie M. Dawley[1], Berit H. Goodge[2,3], Werner Egger[4], Matthew Barone[1], Lena F. Kourkoutis[2,3], David J. Keeble[5], and Darrell G. Schlom[1,3]

1. Department of Materials Science and Engineering, Cornell University, Ithaca, New York 14853, USA

2. School of Applied and Engineering Physics, Cornell University, Ithaca, New York 14853, USA

3. Kavli Institute at Cornell for Nanoscale Science, Ithaca, New York 14853, USA

4. Universität Bundeswehr München, D-85577 Neubiberg, Germany

5. Carnegie Laboratory of Physics, SUPA, School of Science and Engineering, University of Dundee, Dundee DD1 4HN, United Kingdom

Correspondence and requests for materials should be addressed to D.G.S. (email: schlom@cornell.edu)

 This article appeared in *Applied Physics Letters* 117, 062901 (2020) and may be found at https://doi.org/10.1063/5.0011136.

Abstract

The low dielectric loss underlying the record performance of strained $(SrTiO_3)_nSrO$ Ruddlesden-Popper films as tunable microwave dielectrics was postulated to arise from $(SrO)_2$ faults accommodating local non-stoichiometric defects. Here we explore the effect of non-stoichiometry on $(SrTiO_3)_nSrO$ using positron annihilation lifetime spectroscopy on a composition series of 300 nm thick $n = 6$ $(Sr_{1+\delta}TiO_3)_nSrO$ thin films. These films show titanium-site vacancies across the stoichiometry series, with evidence that TiO_x vacancy complexes dominate. Little change in defect populations is observed across the series indicating the ability of Ruddlesden-Popper phases to accommodate ± 5% off-stoichiometry. This ability for defect accommodation is corroborated by scanning transmission electron microscopy with electron energy loss spectroscopy.

Defects play a key role in understanding and engineering materials. In the $n = \infty$ parent phase of the Ruddlesden-Popper $(SrTiO_3)_nSrO$, pure $SrTiO_3$, intrinsic point defects can dramatically affect properties: oxygen-reduced samples induce *n*-type conduction,[1] off-stoichiometric point defects increase thermal conductivity,[2,3] and ferroelectricity can emerge for ultrathin films due to nanopolarized intrinsic point defects.[4] The quantitative prediction,[5,6] identification, and measurement of these defects in $SrTiO_3$ thin films is challenging. For titanium-rich films it is known that there is a corresponding increase in strontium vacancies, titanium antisite defects, and amorphous TiO_2-rich regions.[7-10] For strontium-rich $SrTiO_3$, the defect mechanisms are less well understood. In bulk $SrTiO_3$, $(SrO)_2$ faults are observed with strontium excess of >0.01 at.%,[11,12] forming disordered $(SrTiO_3)_nSrO$ Ruddlesden-Popper phases.[13-15] Ruddlesden-Popper superlattices have gained interest in recent years for their superconducting,[16-19] colossal magnetoresistive,[20] ferroelectric,[21-25] and tunable dielectric,[26,27] properties and use as cathodes in solid fuel cells,[28] without full elucidation of the defect mechanisms in these materials. When epitaxially strained, these superlattice structures have the highest reported figure of merit for high-frequency tunable dielectrics,[26,27] at variance to the high loss seen in their titanate counterparts, $SrTiO_3$, $BaTiO_3$, and $(Ba,Sr)TiO_3$.[29-31] Because loss at these gigahertz frequencies is caused by extrinsic defects, notably charged point defects, high figures of merit indicate their absence in these superlattices.

In $SrTiO_3$, Ruddlesden-Popper non-stoichiometric defects are hypothesized to be accommodated by growth (strontium excess) or reduction (titanium excess) of $(SrO)_2$ planar faults which have a lower formation energy than that of a point defect.[32] Here, using positron annihilation lifetime spectroscopy (PALS), we examine how Ruddlesden-Popper structures accommodate off-stoichiometry when $Sr_{1+\delta}TiO_3$ is inserted into a $n = 6$ $(SrTiO_3)_nSrO$ structure

grown by oxide molecular-beam epitaxy (MBE). We have used PALS previously to examine pulsed-laser deposited (PLD) 200 nm thick titanium-rich $SrTiO_3$ films and found a clear trend in the presence of both strontium and titanium vacancies.[8,9] In titanium-rich $SrTiO_3$ thin films grown homoepitaxially by PLD on (001) $SrTiO_3$ substrates, strontium vacancies were found to dominate, crossing over to a higher proportion of titanium vacancies as the films became more stoichiometric. All films had vacancy concentrations >50 ppm.

Experiment

300 nm thick $n = 6$ $(Sr_{1+\delta}TiO_3)_nSrO$ films with a range of compositions ($\delta = \pm 5\%$) were grown on (001) $SrTiO_3$ single crystal substrates. Films were deposited using a Veeco GEN10 MBE chamber at 900 °C in an oxidant background pressure of 1×10^{-6} Torr O_2 + ~10% O_3. Atomic layering was achieved by elemental source shuttering and calibration of individual SrO and TiO_2 monolayer shutter times using reflection high-energy electron diffraction (RHEED) intensity oscillations.[33-35] Shutter times were then increased or decreased to achieve ± 5% Sr/Ti ratio for off-stoichiometric samples.

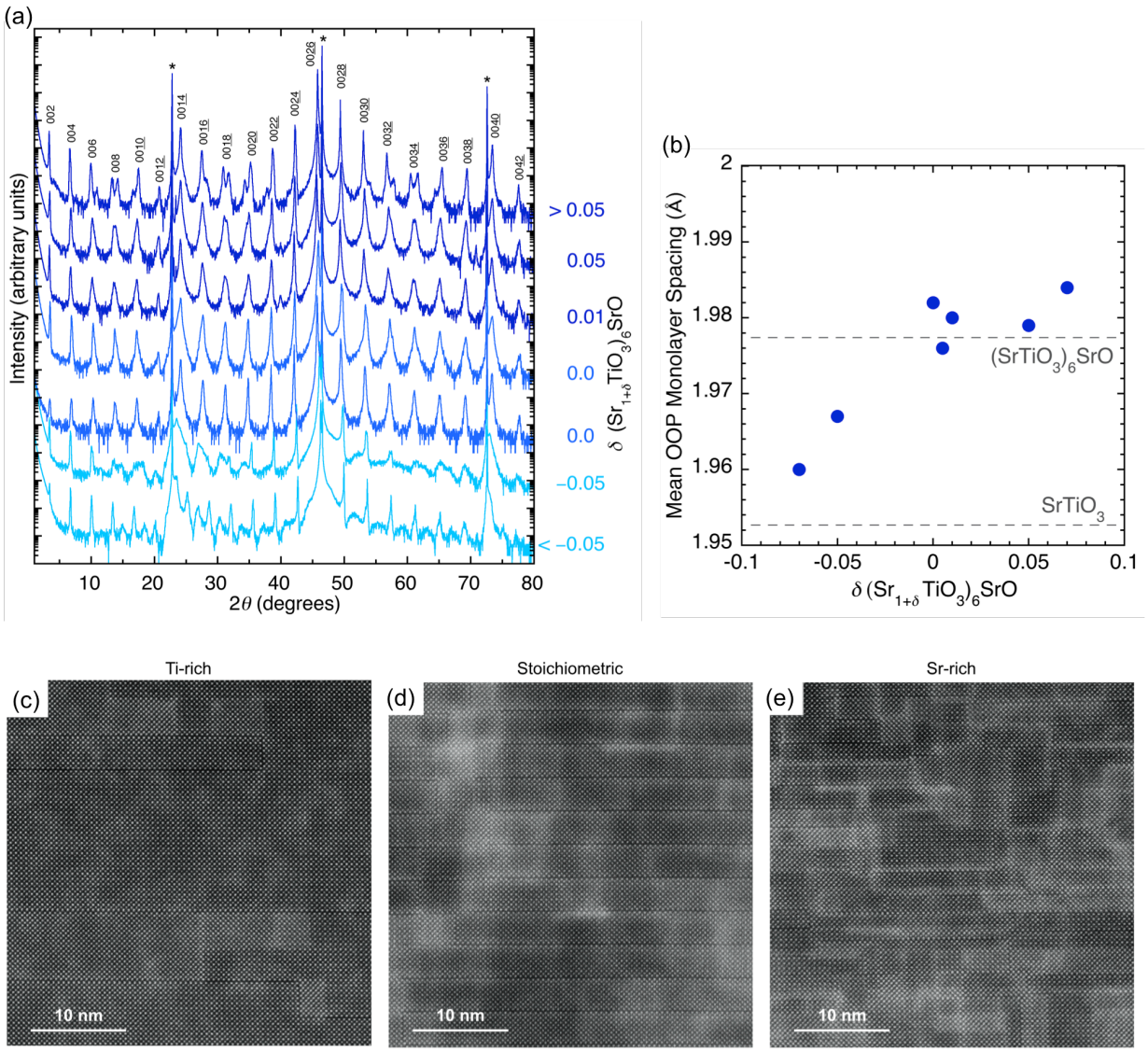

FIG. 1 (a) X-ray diffraction of $\delta = \pm 5\%$ of 300 nm thick $n = 6$ $(Sr_{1+\delta}TiO_3)_nSrO$ films grown on (001) $SrTiO_3$. The diffraction-peak periodicity degrades with increasing off-composition. The (001) $SrTiO_3$ substrate peaks are labeled with an asterisk (*). (b) The mean out-of-plane (OOP) monolayer spacing of $n = 6$ $(Sr_{1+\delta}TiO_3)_nSrO$ films calculated from the 00$\underline{26}$ peak. The y-axis error is the size of the plot markers. (c)-(e) Representative atomic resolution MAADF-STEM images of three $(Sr_{1+\delta}TiO_3)_nSrO$ films show how off-stoichiometry is accommodated structurally through the (c) removal (titanium-rich) or (e) addition (strontium-rich) of SrO planes as compared to (d) a stoichiometric sample.

Samples were characterized by x-ray diffraction as seen in FIG. 1(a). As the films become further off-stoichiometric, the diffraction peaks begin to split, indicating a loss in

superlattice periodicity. This occurs more rapidly for titanium-rich films than strontium-rich. All films have narrow ω rocking curves with full-width-at-half-maximum (FWHM) comparable to the underlying substrate < 34 arcsec (0.009°) (not shown). The low FWHM of these films attests to the defect accommodating nature of $(SrTiO_3)_nSrO$ despite portions of the samples being off-stoichiometric by > 5%. The main superlattice peak, 00$\underline{26}$ is a good measure of the average out-of-plane (OOP) spacing, i.e., the average spacing between SrO and TiO_2 cation layers along the [001] direction, and is plotted in FIG. 1(b).[35] The spacing between two SrO layers is larger than that of a TiO_2 and SrO layer, so higher average monolayer spacing indicates more horizontal SrO layers in the film. The average spacing between monolayers decreases sharply in strontium-deficient (titanium-rich) films due to fewer in-plane $(SrO)_2$ faults. In the strontium-rich regime we do not see the same average monolayer spacing increase, likely because the additional $(SrO)_2$ faults that form are primarily oriented vertically (parallel to the direction of film growth).

Detailed investigation into the structure of these films was conducted with atomic resolution scanning transmission electron microscopy (STEM). Cross-sectional samples of the titanium-rich ($\delta \sim -0.5$), stoichiometric, and strontium-rich ($\delta \sim +0.5$) films seen in FIG. 1(c)-(e) were prepared to a thickness of ~20 nm using the standard focused ion beam (FIB) lift out method on a Thermo Scientific Helios G4 UX FIB. The samples were imaged on an aberration-corrected FEI Titan Themis at 120 kV with a probe convergence semi-angle of 21.4 mrad. Inner and outer collection angles of 36 and 107 mrad, respectively, were used to collect medium-angle annular dark field (MAADF) STEM images, revealing the atomic structure of the films, shown in FIG. 1(c)-(e). In addition to the high-angle *Z*-contrast that distinguishes between heavy and light nuclei, the lower collection angles included in MAADF-STEM also contribute some

diffraction contrast in the resulting images. Signatures of local crystallographic strain fields can be observed where brightening of the background highlights planar defects in the lattice.

Electron energy loss spectroscopy (EELS) mapping was also preformed using the same Titan system equipped with a 965 GIF Quantum ER and Gatan K2 Summit detector operated in electron counting mode, with a beam current of ~30 pA and scan times of 2.5-5 ms per 0.4 Å pixel.

To identify vacancies in the $n = 6$ $(Sr_{1+\delta}TiO_3)_nSrO$ thin-film stoichiometry series, we measured vacancy populations using variable-energy positron annihilation lifetime spectroscopy (VE-PALS). Positrons implanted in the films rapidly thermalize and then annihilate with a bulk lattice or defect state, with a characteristic lifetime τ_i, and probability I_i. The positron annihilation event emits two simultaneous γ-rays, one of which is detected. The time intervals with respect to the arrival of the positrons form the lifetime spectrum. By analyzing the lifetime spectrum, the positron lifetime components characteristic of the bulk (perfect lattice) or defect states are extracted. The positron trapping probability of a defect depends on its charge and open volume size; more negatively charged vacancy defects, such as strontium and titanium vacancies, trap more strongly. VE-PALS measurements were performed on the $n = 6$ $(Sr_{1+\delta}TiO_3)_nSrO$ films using the neutron induced positron beamline (NEPOMUC) operated by FRM II at the Heinz Maier-Leibnitz Zentrum (MLZ), Garching.[36,37] The positron lifetime spectra were measured using position implantation energies of 5 or 6 keV, giving a calculated mean implantation depth of 100 - 140 nm in $SrTiO_3$.[8,9] The spectrometer was set to have a 40 ns time window and each spectrum contained 4×10^6 counts. From a four-term free fit of the resulting spectra the dominant state is shown for each film in FIG. 2 compared to the characteristic lifetime of possible $SrTiO_3$

vacancy states as calculated in Refs. 8 and 38, and from defect structures reported in Ref. 39 (also see Supplementary Information) using the MIKA/DOPPLER package.[40]

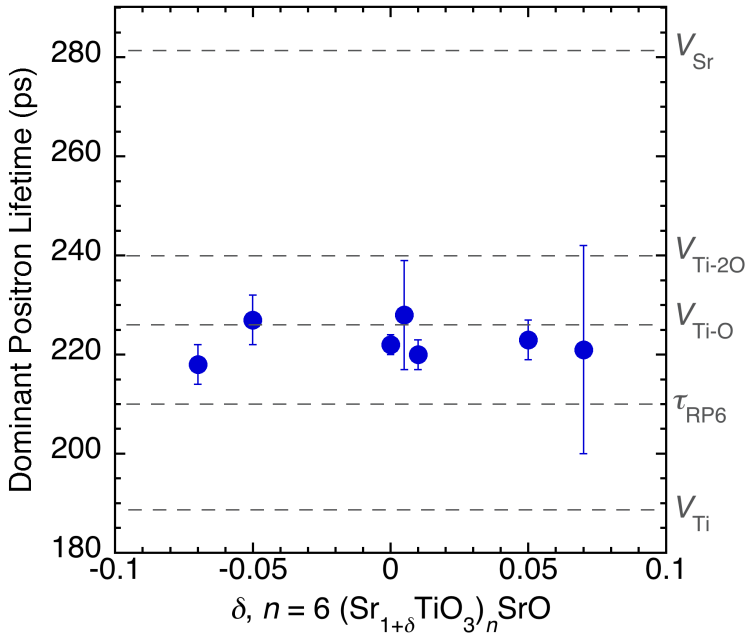

FIG. 2 The dominant positron lifetime from a free fit of the PALS spectra of the $n = 6$ $(Sr_{1+\delta}TiO_3)_nSrO$ thin-film stoichiometry series. Dashed lines show the characteristic lifetimes associated with possible defects in $SrTiO_3$ and τ_{RP6}, the bulk lifetime for $n = 6$ $(SrTiO_3)_nSrO$.

Discussion

If $(SrO)_2$ Ruddlesden-Popper faults do not accommodate off-stoichiometry we would expect the titanium rich-films, $\delta < 0$, to have higher strontium vacancy concentrations which would produce a high dominant positron lifetime in the range 280 – 290 ps as seen in Refs. 8-9. In contrast, dominant lifetimes for the $n = 6$ $(Sr_{1+\delta}TiO_3)_nSrO$ films show little variance and are clustered between 218 – 230 ps (FIG. 3), around the TiO_x vacancy lifetimes, contributing > 70% of the total spectra intensity (see Supplementary Table 1). While it is non-trivial to distinguish the contribution of each V_{TiOx} state and the bulk state of pure $(SrTiO_3)_6SrO$, τ_{RP6}, it is clear that V_{TiOx} is the dominant vacancy found in $n = 6$ $(Sr_{1+\delta}TiO_3)_nSrO$. When a four-term fit of the spectra

is forced to include V_{Ti} or V_{Sr} (see Supplementary Table 1), a free term is still found between 198 – 266 ps, intermediate between the V_{Ti} and V_{Sr} values, indicating that the dominant lifetime component is not solely a convolution of titanium and strontium vacancies as found in our previous measurements on PLD $SrTiO_3$ films.[8,9]

The titanium-oxygen vacancy complexes, TiO_x, identified by our PALS results are likely charge neutral and explain the low loss properties of these tunable dielectric materials at high frequency. In the case of TiO_2 ($x = 2$) vacancies, they are charge neutral and in essence regions of $(SrO)_2$ faults, seen as $SrTiO_3 + V_{TiO2} = SrO$.[41] If they exist, vacancies of TiO ($x = 1$), are also likely charge neutral with the addition of two electrons from nearby oxygen vacancies.[42] These results establish the ability of the $(SrTiO_3)_nSrO$ structure to mitigate defects and explain the exceptional performance of strained $(SrTiO_3)_nSrO$ films at gigahertz frequencies where loss has been identified to be due to charged point defects.[29-31]

The structural accommodations revealed by STEM-EELS support this interpretation of the PALS data. Dark boundaries between SrO planes in FIGs. 1(c)-(e) and 4 can easily be traced between regions of continuous perovskite, most notably as the boundaries between the $n = 6$ Ruddlesden-Popper layers. In general, atomic columns of strontium and titanium can be differentiated by their relative brightness, with heavy strontium atoms appearing brighter than comparatively lighter titanium sites. Areas where all atomic sites show similar contrast suggest projection through atomic columns containing both strontium and titanium, indicating regions which are crystallographically offset by $\frac{a}{2}[110]$ due to an $(SrO)_2$ Ruddlesden-Popper fault.

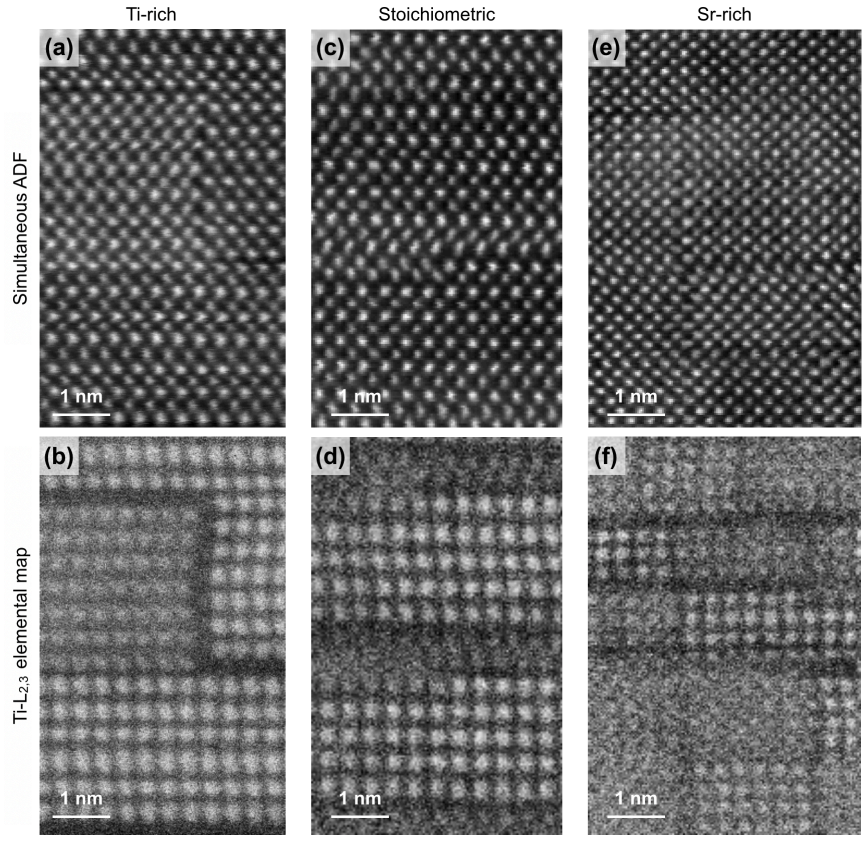

FIG. 3 Atomic-resolution EELS mapping of the Ti-$L_{2,3}$ edge highlights how the Ruddlesden-Popper structure ((c) and (d)) adapts to accommodate off-stoichiometry by forming (a) and (b) larger (titanium-rich) or (e) and (f) smaller (strontium-rich) blocks of continuous $SrTiO_3$ between SrO plane boundaries.

In the stoichiometric case, FIG. 1(d) and 3(d), discrete $(SrO)_2$ layers are separated by clear gaps in the titanium elemental map where SrO planes form rock salt boundaries. The nominally stoichiometric film displays general adherence to the $n = 6$ Ruddlesden-Popper structure, though some disruptions are observed as inclusions of vertical SrO planes and subtle crystalline defects like the step edge shown here.

The titanium-rich (strontium-poor) film in FIG. 1(c) and 4(b) shows how the Ruddlesden-Popper phase has adjusted to accommodate its off-stoichiometry: larger regions of continuous $SrTiO_3$ have formed as excess titanium fills in between neighboring SrO rock salt layers (or,

equivalently, as SrO rock salt boundaries are removed). The elemental map in FIG. 3(b) clearly shows regions of both higher *n* (upper right corner) as well as projection through an $(SrO)_2$ Ruddlesden-Popper fault along the growth direction (central region).

In contrast, the strontium-rich film in FIG. 1(e) and 3(f) forms extra SrO planes beyond the normal Ruddlesden-Popper phase, breaking up the $n = 6$ layers both horizontally and vertically into regions of locally smaller effective *n*, similar to effects observed in other strontium-rich $SrTiO_3$ films.[43] The titanium map of the strontium-rich film, FIG. 3(f), provides a clear view of extra SrO planes forming both vertically and horizontally, dividing Ruddlesden-Popper layers into "bricks" of much smaller effective *n*.

Conclusion

The defect mitigating nature of $(SrTiO_3)_nSrO$ Ruddlesden-Popper phases was probed with PALS by introducing off-stoichiometric $Sr_{1+\delta}TiO_3$ into the Ruddlesden-Popper superlattice to form a series of 300 nm thick $n = 6$ $(Sr_{1+\delta}TiO_3)_nSrO$ thin films grown by MBE on (001) $SrTiO_3$. Atomic resolution STEM and EELS show how off-stoichiometric films adjust structurally to accommodate either excess titanium (fewer SrO rock salt boundaries) or excess strontium (additional SrO rock salt boundaries). The lack of variance with off-stoichiometry seen in corresponding PALS spectra, and the absence of trapping to strontium vacancies in titanium-rich films, further supports this conclusion that $(SrO)_2$ faults are indeed accommodating non-stoichiometry without dominant introduction of cation monovacancies as observed in PLD $Sr_{1+\delta}TiO_3$ thin films.[8,9] The observed TiO_x vacancies are likely charge neutral nano-regions of SrO faults, $SrTiO_3 + V_{TiO} = SrO$. Further studies of the contribution of oxygen vacancies and antisite defects which cannot be fully studied with PALS are needed to provide full understanding of the defect mechanisms in $(SrTiO_3)_nSrO$.

Acknowledgments

The synthesis science work at Cornell was supported by the U.S. Department of Energy, Office of Basic Sciences, Division of Materials Sciences and Engineering, under Award No. DE-SC0002334. Sample preparation was in part facilitated by the Cornell NanoScale Facility, a member of the National Nanotechnology Coordinated Infrastructure (NNCI), which is supported by the National Science Foundation (Grant NNCI-1542081). This work made use of Cornell Center for Materials Research Shared Facilities, which are supported through the NSF MRSEC program (DMR-1719875). B.H.G. and L.F.K. acknowledge support by the Department of Defense Air Force Office of Scientific Research (No. FA 9550-16-1-0305). The FEI Titan Themis 300 was acquired through No. NSF-MRI-1429155, with additional support from Cornell University, the Weill Institute, and the Kavli Institute at Cornell. The Helios G4 X FIB was acquired with support by NSF Platform for Accelerated Realization, Analysis, and Discovery of Interface Materials (PARADIM) (DMR-1539918). D.J.K. gratefully acknowledge the financial support provided by FRM-II to perform the neutron scattering measurements at the Heinz Maier-Leibnitz Zentrum (MLZ), Garching, Germany

AIP Publishing Data Sharing Policy

The data that support the findings of this study are available in the supplementary information or from the corresponding author upon reasonable request.

References

1. H. Yamada and G. R. Miller, J. Solid State Chem. **6**, 169 (1973).

2. S. Wiedigen, T. Kramer, M. Feuchter, I. Knorr, N. Nee, J. Hoffmann, M. Kamlah, C. A. Volkert, and Ch. Jooss, Appl. Phys. Lett. **100**, 061904 (2012).

3. C. M. Brooks, R. B. Wilson, A. Schäfer, J. A. Mundy, M. E. Holtz, D. A. Muller, J. Schubert, D. G. Cahill, and D. G. Schlom, Appl. Phys. Lett. **107**, 051902 (2015).

4. D. Lee, H. Lu, Y. Gu, S.-Y. Choi, S.-D. Li, S. Ryu, T. R. Paudel, K. Song, E. Mikheev, S. Lee, S. Stemmer, D. A. Tenne, S. H. Oh, E. Y. Tsymbal, X. Wu, L.-Q. Chen, A. Gruverman, and C. B. Eom, Science **349**, 1314 (2015).

5. T. Tanaka, K. Matsunaga, Y. Ikuhara, and T. Yamamoto, Phys. Rev. B **68**, 205213 (2003).

6. D. Freedman, D. Roundy, and T. Arias, Phys. Rev. B **80**, 064108 (2009).

7. T. Suzuki, Y. Nishi and M, Fujimoto, Philos. Mag. A **80**, 621 (2000).

8. D. J. Keeble, S. Wicklein, R. Dittmann, L. Ravelli, R. A. Mackie, and W. Egger, Phys. Rev. Lett. **105**, 226102 (2010).

9. D. J. Keeble, S. Wicklein, L. Jin, C. L. Jia, W. Egger, and R. Dittmann, Phys. Rev. B **87**, 195409 (2013).

10. D. Lee, H. Wang, B. A. Noesges, T. J. Asel, J. Pan, J.-W. Lee, Q. Yan, L. J. Brillson, X. Wu, and C.-B. Eom, Phys. Rev. Mater. **2**, 060403 (2018).

11. S. Witek, D. M. Smyth, and H. Pickup, J. Am. Ceram. Soc. **67**, 372 (1984).

12. L. J. Knott, N. J. Cockroft, and J. C. Wright, Phys. Rev. B **51**, 5649 (1995).

13. D. Balz and K. Plieth, Z. Electrochem. **59**, 545 (1955).

14. S. N. Ruddlesden and P. Popper, Acta Crystallogr. **10**, 538 (1957).

15. S. N. Ruddlesden and P. Popper, Acta Crystallogr. **11**, 54 (1958).

16. J. G. Bednorz and K. A. Müller, Z. Phys. B **64**, 189 (1986).

17. H. M. Buschbaum, Angew. Chem. Int. Ed. **28**, 1472 (1989).

18. Y. Maeno, H. Hashimoto, K. Yoshida, S. Nishizaki, T. Fujita, J. G. Bednorz, and F. Lichtenberg, Nature **372**, 532 (1994).

19. T. L. Meyer, R. Jacobs, D. Lee, L. Jiang, J. W. Freeland, C. Sohn, T. Egami, D. Morgan, and H. N. Lee, Nature Commun. **9**, 92 (2018).

20. Y. Moritomo, A. Asamitsu, H. Kuwahara, and Y. Tokura, Nature **380**, 141 (1996).

21. T. Birol, N. A. Benedek, and C. J. Fennie, Phys. Rev. Lett. **107**, 257602 (2011).

22. M. J. Pitcher, P. Mandal, M. S. Dyer, J. Alaria, P. Borisov, H. Niu, J. B. Claridge, and M. J. Rosseinsky, Science **347**, 420 (2015).

23. Y. S. Oh, X. Luo, F.-T. Huang, Y. Wang, and S.-W. Cheong, Nat. Mater. **14**, 407 (2015).

24. N. A. Benedek, J. M. Rondinelli, H. Djani, P. Ghosez, and P. Lightfoot, Dalton Trans. **44**, 10543 (2015).

25. P. V. Balachandran, J. Young, T. Lookman, and J. M. Rondinelli, Nat. Commun. **8**, 14282 (2017).

26. C.-H. Lee, N. D. Orloff, T. Birol, Y. Zhu, V. Goian, E. Rocas, R. Haislmaier, E. Vlahos, J. A. Mundy, L. F. Kourkoutis, Y. Nie, M. D. Biegalski, J. Zhang, M. Bernhagen, N. A. Benedek, Y. Kim, J. D. Brock, R. Uecker, X. X. Xi, V. Gopalan, D. Nuzhnyy, S. Kamba, D. A. Muller, I. Takeuchi, J. C. Booth, C. J. Fennie, and D. G. Schlom, Nature **502**, 532 (2013).

27. N. M. Dawley, E. J. Marksz, A. M. Hagerstrom, G. H. Olsen, M. E. Holtz, V. Goian, C. Kadlecch, J. Zhang, X. Lu, J. A. Drisko, R. Uecker, S. Ganschow, C. J. Long, J. C. Booth, S. Kamba, C. J. Fennie, D. A. Muller, N. D. Orloff, and D. G. Schlom, Nat. Mater. **19**, 176 (2020).

28. G. Amow, I. J. Davidson, and S. J. Skinner, Solid State Ionics **177**, 1205 (2006).

29. C. Elissalde, and J. Ravez, J. Mater. Chem. **11**, 1957 (2001).

30. A. K. Tagantsev, V. O. Sherman, K. F. Astafiev, J. Venkatesh, and N. Setter, J. Electroceram. **11**, 5 (2003).

31. A. Vorobiev, P. Rundqvist, K. Khamchane, and S. Gevorgian, J. Appl. Phys. **96**, 4642 (2004).

32. M. A. Mccoy, R. W. Grimes, and W. E. Lee, Philos. Mag. A **75**, 833 (1997).

33. J. H. Haeni, C. D. Theis, and D. G. Schlom, J. Electroceram. **4**, 385 (2000).

34. R. C. Haislmaier, G. Stone, N. Alem, and R. Engel-Herbert, Appl. Phys. Lett. **109**, 043102 (2016).

35. M. Barone, N. M. Dawley, H. Nair, M. Holtz, A. Soukiassian, K. Lee, Y. Jia, T. Heeg, R. Gatt, Y. Nie, and D. G. Schlom, (unpublished).

36. P. Sperr, W. Egger, G. Kogel, G. Dollinger, C. Hugenschmidt, R. Repper, and C. Piochacz, Appl. Surf. Sci. **255**, 35 (2008).

37. C. Hugenschmidt, B. Lowe, J. Mayer, C. Piochacz, P. Pikart, R. Repper, M. Stadlbauer, and

K. Schreckenbach, Nucl. Instrum. Methods A **593**, 616 (2008).

38. D. J. Keeble, R. A. Mackie, W. Egger, B. Löwe, P. Pikart, C. Hugenschmidt, and T. J. Jackson, Phys. Rev. B **81**, 064102 (2010).

39. T. Tanaka, K. Matsunaga, Y. Ikuhara, and T. Yamamoto, Phys. Rev. B **68**, 205213 (2003).

40. T. Torsti, T. Eirola, J. Enkovaara, T. Hakala, P. Havu, V. Havu, T. Hoynalanmaa, J. Ignatius, M. Lyly, I. Makkonen, T. T. Rantala, J. Ruokolainen, K. Ruotsalainen, E. Rasanen, H. Saarikoski, and M. J. Puska, Phys. Status Solidi B **243**, 1016 (2006).

41. U. Balachandran and N. G. Eror, J. Mater. Sci. **17**, 2133 (1982).

42. A. Janotti, J. B. Varley, M. Choi, and C. G. Van de Walle, Phys. Rev. B **90**, 085202 (2014).

43. C. M. Brooks, L. Fitting Kourkoutis, T. Heeg, J. Schubert, D. A. Muller, and D. G. Schlom, Appl. Phys. Lett. **94**, 162905 (2009).